01 Feb 2016

Neutron and Magnetic Studies of $La_{0.7}Sr_{0.3}Mn_{1-x}Cr_xO_3$ ($x \leq 0.7$): A Homogeneous Charge-Ordered System

Thomas F. Creel

Jinbo Yang

Satish K. Malik

Sylvio Quezado

et. al. For a complete list of authors, see https://scholarsmine.mst.edu/phys_facwork/747

Recommended Citation

T. F. Creel et al., "Neutron and Magnetic Studies of $La_{0.7}Sr_{0.3}Mn_{1-x}Cr_xO_3$ ($x \leq 0.7$): A Homogeneous Charge-Ordered System," *Physical review B: Condensed matter and materials physics*, vol. 93, no. 8, American Physical Society, Feb 2016.
The definitive version is available at https://doi.org/10.1103/PhysRevB.93.085116

Neutron and magnetic studies of $La_{0.7}Sr_{0.3}Mn_{1-x}Cr_xO_3 (x \leqslant 0.7)$: A homogeneous charge-ordered system

Thomas F. Creel,[1,*] Jinbo Yang,[2] Satish K. Malik,[3] S. Quezado,[3] O. A. Pringle,[1] William B. Yelon,[4] and William J. James[4]

[1]*Department of Physics, Missouri University of Science and Technology, Rolla, Missouri 65409, USA*

[2]*State Key Laboratory for Artificial Microstructure, Mesoscopic Physics and School of Physics, Peking University, Beijing*

[3]*Departamento de Física Teórica e Experimental (DFTE), Universidade Federal do Rio Grande do Norte (UFRN), Natal, Brazil*

[4]*Department of Chemistry, Graduate Center for Materials Research, Missouri University of Science and Technology, Rolla, Missouri 65409, USA*

(Received 15 February 2015; published 10 February 2016)

Structural and magnetic properties of $La_{0.7}Sr_{0.3}Mn_{1-x}Cr_xO_3$ ($0 < x \leqslant 0.7$) have been studied in order to determine the effect of substitution of Cr^{3+} for Mn^{3+}. The data consist of neutron and x-ray powder-diffraction and magnetization measurements. We previously suggested these systems transition from ferromagnetic to antiferromagnetic ordering with the intermediate concentrations containing coexisting ferromagnetic and antiferromagnetic domains. Upon further detailed examination, we find that the neutron data can be fit using a single homogeneous long-range magnetically ordered state and compositionally dependent charge ordering. The magnetic structures are controlled by the competition between Mn-Mn, Mn-Cr, and Cr-Cr interactions (double exchange and superexchange). The metal to semimetal and semimetal to insulator transitions can be quantitatively described as due to the localization effect of superexchange. The presence of charge ordered states in the insulating region arises from the favorable energetics of Mn^{4+}-O-Cr^{3+} superexchange bonds relative to Mn^{3+}-O-Cr^{3+} bonds.

DOI: 10.1103/PhysRevB.93.085116

I. INTRODUCTION

The $LaMnO_3$ perovskites continue to be of significant interest due to their temperature-dependent electronic and magnetic phases. *A*-site (La-site) and *B*-site (Mn-site) doping causes complex compositionally dependent magnetic behavior. These perovskites are known for the unusually large effect that an external magnetic field has on electrical and heat transport [1,2] and interesting metal-insulator transitions associated with the ferromagnetic to paramagnetic transition [3]. Applications of these mixed-valence perovskites include cathodes for solid oxide fuel cells, magnetic storage devices, magnetoresistive read heads, catalysts, colossal magnetoresistance, and giant magnetoresistence materials [4–6]. The underlying mechanism of the magnetic and transport properties of these manganites has been attributed to double exchange, superexchange, semicovalent exchange, Jahn-Teller distortions, and electron-phonon couplings [7–14].

$LaMnO_3$ is antiferromagnetic at low temperatures with $T_N \sim 150$ K [15], crystallizing in the orthorhombic space group *Pbnm*. Oxygen stoichiometry is extremely important, influencing the Jahn-Teller distorted oxygen octahedron surrounding the d^4 Mn^{3+} cation [16].

Substituting divalent Sr^{2+} for trivalent La^{3+} creates *d*-electron holes by oxidizing Mn^{3+} to Mn^{4+} as described by the formula $La^{3+}_{1-x}Sr^{2+}_x(Mn^{4+}_xMn^{3+}_{1-x})O^{2-}_3$. The Curie temperature varies with Mn^{4+} concentration and is controlled by temperature-dependent ferromagnetic and antiferromagnetic couplings [17]. Shirane *et al.* [18] found $La_{0.7}Sr_{0.3}MnO_3$ to be a ferromagnetic metal with $T_C \sim 378$ K and a magnetic moment per Mn of about $3.6\mu_B$. This is in good agreement with the calculated value of $3.7\mu_B$/f.u. (f.u. represents formula unit) assuming complete spin alignment of the magnetic moments of the Mn ions; $4\mu_B$ for Mn^{3+} and $3\mu_B$ for Mn^{4+} [15].

Previous studies substituting Cr on the *B* site while substituting Sr^{2+} for La^{3+} on the *A* site found the Cr ion to be Cr^{3+}, leading to $La^{3+}_{1-x}Sr^{2+}_xMn^{4+}_x(Cr^{3+}_yMn^{3+}_{1-x-y})O^{2-}_3$ [19–22]. X-ray diffraction and magnetic and magnetoresistance measurements indicate that T_C and the lattice parameter *a* decrease with increasing Cr content [22,23]. At low temperatures with less than about 14% Cr, the system is metallic; between ~14% and ~20%, the system is semimetallic whereas for Cr concentrations above ~20% the system is insulating [23,24]. The large difference in magnetization between field-cooled (M_{FC}) and zero-field-cooled (M_{ZFC}) magnetic measurements at low temperatures has been ascribed to ferromagnetic and antiferromagnetic regions or spin or cluster glass [25,26]. The substitution of Cr^{3+} results in antiferromagnetic Cr^{3+}-O^{2-}-Cr^{3+} and Cr^{3+}-O^{2-}-Mn^{4+} interactions and ferromagnetic Cr^{3+}-O^{2-}-Mn^{3+} interactions as predicted by superexchange rules [20,27]. Contradictory models for the alignment of Mn^{3+} ($4\mu_B$), Mn^{4+} ($3\mu_B$), and Cr^{3+} ($3\mu_B$) have been proposed [24,28,29]. For concentrations between 20% and 60%, magnetic order has been interpreted as coexisting ferromagnetic and antiferromagnetic domains or as cluster or spin glass [19,20,25,26,28,29].

In this study, Mn is replaced with up to 70% Cr yielding $La^{3+}_{0.7}Sr^{2+}_{0.3}Mn^{4+}_{0.3}(Cr^{3+}_yMn^{3+}_{0.7-y})O^{2-}_3$, assuming Cr to be in the Cr^{3+} state; an assumption proved in this paper. Neutron diffraction, x-ray diffraction, and magnetic measurements are used to study the nuclear and magnetic structures and magnetic properties of the Cr-substituted perovskite. The temperature and composition dependence of the magnetic structure are determined.

II. EXPERIMENT

Polycrystalline samples of $La^{3+}_{0.7}Sr^{2+}_{0.3}Mn^{4+}_{0.3}(Cr^{3+}_xMn^{3+}_{0.7-x})O^{2-}_3$ ($0 < x \leqslant 0.7$) were prepared by a conventional solid-state reaction method in air. Appropriate

*Corresponding author: tfcbqb@mst.edu

amounts of high purity La_2O_3, $SrCO_3$, MnO_2, and Cr_2O_3 powders were weighed and mixed according to the desired stoichiometry. The samples were ground using a high-energy ball mill for 5 h, pressed into pellets at 10 000 psi, and then fired at 1350 °C for 24 h in air followed by a room-air quench. After 24 h of cooling, the samples were reground, pressed, and fired using the same process.

Neutron powder-diffraction data were collected at 12 and 300 K at the University of Missouri Research Reactor facility using a position sensitive detector diffractometer with a neutron wavelength of $\lambda = 1.479$ Å. X-ray diffraction data were collected with an XPERT PRO diffractometer using a Cu $K\alpha$ wavelength of $\lambda = 1.5481$ Å. The data were refined using the FULLPROF suite of programs [30]. Magnetic measurements were performed at the University of Brasilia using a vibrating sample magnetometer and a Quantum Design physical property measurement system with the ac magnetization option.

III. NEUTRON-DIFFRACTION STUDIES

Refinements of x-ray diffraction data indicate all samples are single phase and crystallize in a rhombohedral structure (space group $R\bar{3}c$, No. 167). The magnetic cell used in the neutron refinements was ($P\bar{1}$) with six B-site (Mn,Cr) positions in a hexagonally unique dual-layered configuration with three $B1$ sites at (0,0,0), (2/3,1/3,1/3), and (1/3,2/3,2/3) and three $B2$ sites at (0,0,1/2), (2/3,1/3,5/6), and (1/3,2/3,1/6). Eleven samples were prepared with nominal Cr content of 5%, 10%, 15%, 20%, 25%, 40%, 50%, 60%, 70%, and two samples at 30% (as measured by weight and calculated by mol %). Neutron-scattering data were collected at 12 and 300 K for each sample and were initially refined using neutron diffraction without including any magnetic phases. The stoichiometry refinements yielded values of 4.2%, 6.2%, 14.3%, 19.6%, 22.1%, 41.1%, 48.5%, and 57.9% for the first eight samples and 29.4% and 36.5% for the two nominal 30% concentrations. The 70% sample was found to have a combination of two phases, likely due to reaching solid solubility limits. Therefore, no further data will be presented in this paper on that sample. Figure 1 shows the neutron-scattering data at 12 K from which data collected at 300 K have been subtracted for all samples. The 12–300-K difference curves emphasize the temperature-dependent changes due to magnetic order. The large positive and negative swings for the (202), (006), and (024) reflections are due to temperature-driven shifts in peak positions. Significant reductions in the intensities of the (012), (110), and the (104) reflections are observed with increasing Cr content. Two new magnetic peaks (113) and (003) + (011) are clearly visible for $x \geqslant 0.196$ in Fig. 1. All samples show resolution limited peaks consistent with long-range magnetic order. The peaks not indexed are associated with the $MnCr_2O_4$ contaminant phase.

The refinement results are presented in Table I. The nominal and refined Cr contents for the ten samples as well as the concentration of the impurity phase $MnCr_2O_4$ are provided. For the remainder of this discussion, we refer to the refined stoichiometries. The lattice parameters decrease with increasing Cr content as expected as Cr^{3+} has an ionic radius of 0.615 Å, slightly smaller than 0.656 Å for Mn^{3+} [31]. The oxygen stoichiometry remains constant within 1σ. For $x > 0.143$, the magnetic moments μ_{B1} and μ_{B2} refer to the refined average moments of the transition-metal atoms (B_1 and B_2 sites) in each layer.

For $x < 0.196$, the samples are simple ferromagnets with magnetic moments that decrease with increasing Cr content and only one moment is presented. Figure 2 shows the neutron scattering (red dots) and refined neutron scattering (black line) for the combined nuclear and magnetic phases for the $x = 0.042$ sample. The insets in Fig. 2 show the observed and fitted data obtained with the best magnetic and nuclear model (left) and nuclear-only model (right). The misfits (right) highlight the magnetic contributions to the (012) and (110) + (104) peaks that are fit by a simple ferromagnetic model (left). This refinement is typical of the refinements for $x < 0.196$. The small peaks at ~17° and 35° are due to the $MnCr_2O_4$ impurity phase.

At 12 K for $0.196 \leqslant x \leqslant 0.411$, the (104) + (110) reflections are still dominant, but two new peaks, inconsistent with a simple ferromagnetic solution emerge (Fig. 1). The [(003) + (011)] peak is purely magnetic, whereas the (113) peak has nuclear and magnetic components. These peaks have led others to hypothesize that the system is inhomogeneous, containing both ferromagnetic and antiferromagnetic components [32]. However, the data can be fit with a single magnetic phase having unequal ferromagnetically aligned moments on the $B1$ and $B2$ sites. Since it is assumed that the Mn and Cr concentrations on all B sites are random, the unequal moments on the $B1$ and $B2$ sites for $x > 0.196$ must arise through charge ordering, which creates higher and lower Mn^{4+} concentrations on the different layers.

Figure 3 shows the neutron-scattering data for the $x = 0.579$ sample at 12 K. The (104) + (110) reflections are present but weak whereas the (003) + (011) reflections are now dominant. The insets in Fig. 3 show the observed and fitted data using the best nuclear-only model. We find unequal moments, antiferromagnetically aligned in the B_1 and B_2 layers.

Figure 4 shows magnified regions where magnetic peaks are observed (left) and magnetic ordering schema (right) for three different samples that correspond to the three

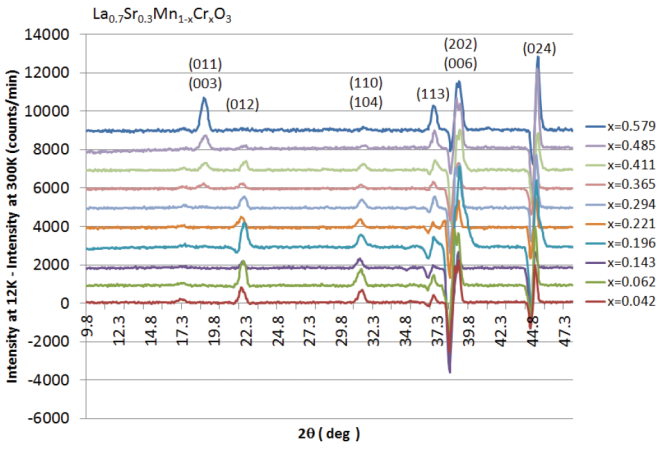

FIG. 1. Intensity versus scattering angle of neutron-scattering data collected at 300 K subtracted from data collected at 12 K for all Cr-substituted concentrations. Successive concentrations are offset by 1000 counts.

TABLE I. Refined parameters: magnetic moment (μ_B), a, c, volume, χ^2, and contaminant ($MnCr_2O_4$) phase versus nominal and refined Cr content. The magnetic moments are calculated on the B sites and represent the average for the three species on those sites. The numbers in parentheses represent the uncertainty in the last digit. Columns labeled μ_{B1} and μ_{B2} are magnetic moments for the $B1$ and $B2$ sites for $x > 0.143$. In the last column where no moments are listed on the $B2$ sites, no extra reflections are seen. The Cr and $MnCr_2O_4$ contents were refined at room temperature.

	Nominal Cr content (mol %)	Refined Cr content (mol %)	$MnCr_2O_4$ content (mol %)	a (Å)	c (Å)	Cell volume (Å)^3	χ^2	O^{-2} stoichiometry	$\mu_{B1,Mn}$ (μ_B)	$\mu_{B2,Mn}$ (μ_B)
12 K	5	4.2	1.6	5.4906 (1)	13.3112 (1)	347.53 (2)	3.31	3.1 (1)	3.13 (3)	
	10	6.2	1.2	5.4909 (1)	13.3027 (5)	347.34 (2)	5.47	3.1 (1)	2.95 (4)	
	15	14.3	1.5	5.4905 (2)	13.3046 (5)	347.33 (2)	3.11	3.0 (0)	2.48 (4)	
	20	19.6	1.2	5.4873 (1)	13.2914 (3)	346.59 (1)	2.99	3.1 (1)	2.56 (7)	1.97 (7)
	25	22.1	1.6	5.4855 (2)	13.2906 (5)	346.34 (2)	3.75	3.0 (0)	1.8 (1)	2.3 (1)
	30	29.4	2.2	5.4853 (1)	13.2905 (4)	346.31 (2)	3.00	3.1 (1)	1.29 (5)	2.24 (6)
	30	36.5	2.7	5.4798 (2)	13.2858 (4)	345.50 (2)	2.63	3.1 (1)	0.53 (6)	2.63 (7)
	40	41.1	2.3	5.4786 (2)	13.2883 (5)	345.41 (2)	3.11	2.9 (1)	0.60 (6)	2.79 (7)
	50	48.5	2.4	5.4757 (1)	13.2669 (3)	344.50 (1)	2.30	3.0 (0)	−0.8 (1)	2.1 (1)
	60	57.9	3.6	5.4693 (2)	13.2641 (4)	343.62 (2)	3.80	2.9 (1)	−1.7 (3)	2.2 (3)
300 K	5	4.2	1.6	5.4982 (1)	13.3496 (4)	349.50 (2)	2.85	3.1 (1)	2.16 (3)	
	10	6.2	1.2	5.4987 (1)	13.3416 (5)	349.35 (2)	4.58	3.1 (1)	1.65 (4)	
	15	14.3	1.5	5.4967 (1)	13.3391 (5)	349.03 (2)	2.86	3.0 (0)	0.64 (7)	
	20	19.6	1.2	5.4939 (2)	13.3269 (5)	348.37 (2)	4.68	3.1 (1)	0.4 (1)	
	25	22.1	1.6	5.4936 (2)	13.3325 (5)	348.46 (2)	2.88	3.1 (1)	0.00	0.00
	30	29.4	2.2	5.4909 (1)	13.3257 (4)	347.94 (2)	2.57	3.1 (1)	0.00	0.00
	30	36.5	2.7	5.4867 (2)	13.3246 (5)	347.38 (2)	2.65	3.0 (0)	0.00	0.00
	40	41.1	2.3	5.4855 (2)	13.3182 (6)	347.07 (2)	3.05	2.8 (1)	0.00	0.00
	50	48.5	2.4	5.4849 (1)	13.3139 (4)	346.87 (1)	2.09	3.1 (1)	0.00	0.00
	60	57.9	3.6	5.4772 (2)	13.3051 (5)	345.68 (2)	3.22	2.9 (1)	0.00	0.00

different observed magnetic behaviors; $x = 0.048$ [Fig. 4(a)], $x = 0.411$ [Fig. 4(b)], and $x = 0.579$ [Fig. 4(c)]. As Cr increases, the intensity in the (012) and (110) + (104) peaks decreases, whereas the intensity in the (011) + (003) and (113) peaks increases, as the system transitions from a simple ferromagnet ($x < 0.2$) with the same moments on the B_1 and B_2 sites to a layered ferromagnet with different moments on the B_1 and B_2 sites ($0.2 < x \lesssim 0.48$) to a ferrimagnet with opposing unequal moments on the B_1 and B_2 sites ($x \gtrsim 0.48$).

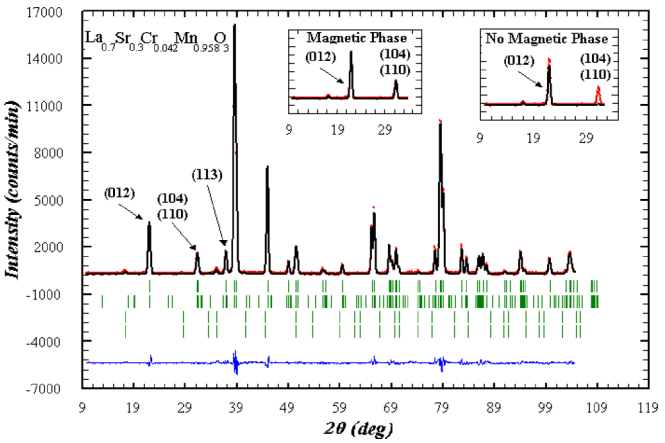

FIG. 2. Neutron-diffraction refinement of the $La_{0.7}Sr_{0.3}Mn_{0.958}Cr_{0.042}O_3$ sample at 12 K. The reflection markers below the plot are, in order, nuclear perovskite structure, ferromagnetic perovskite structure, and nuclear and magnetic structures for $MnCr_2O_4$. The small peak intensities at ∼17° and 35° are due to the $MnCr_2O_4$ phase. The insets show the magnified regions around the (012) and the (104) + (110) reflections prior to the addition of the magnetic phase (right) and after the magnetic phase (left) was added to the refinement.

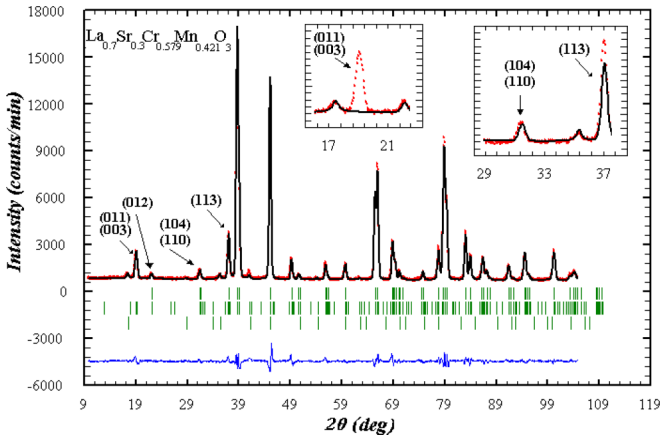

FIG. 3. Neutron-diffraction refinement of the $La_{0.7}Sr_{0.3}Mn_{0.421}Cr_{0.579}O_3$ sample at 12 K. The Bragg reflection markers below the plot are in order nuclear perovskite structure, magnetic perovskite structure, and $MnCr_2O_4$ nuclear structure. The insets show the magnified regions around the two magnetic peaks prior to the addition of the magnetic phase.

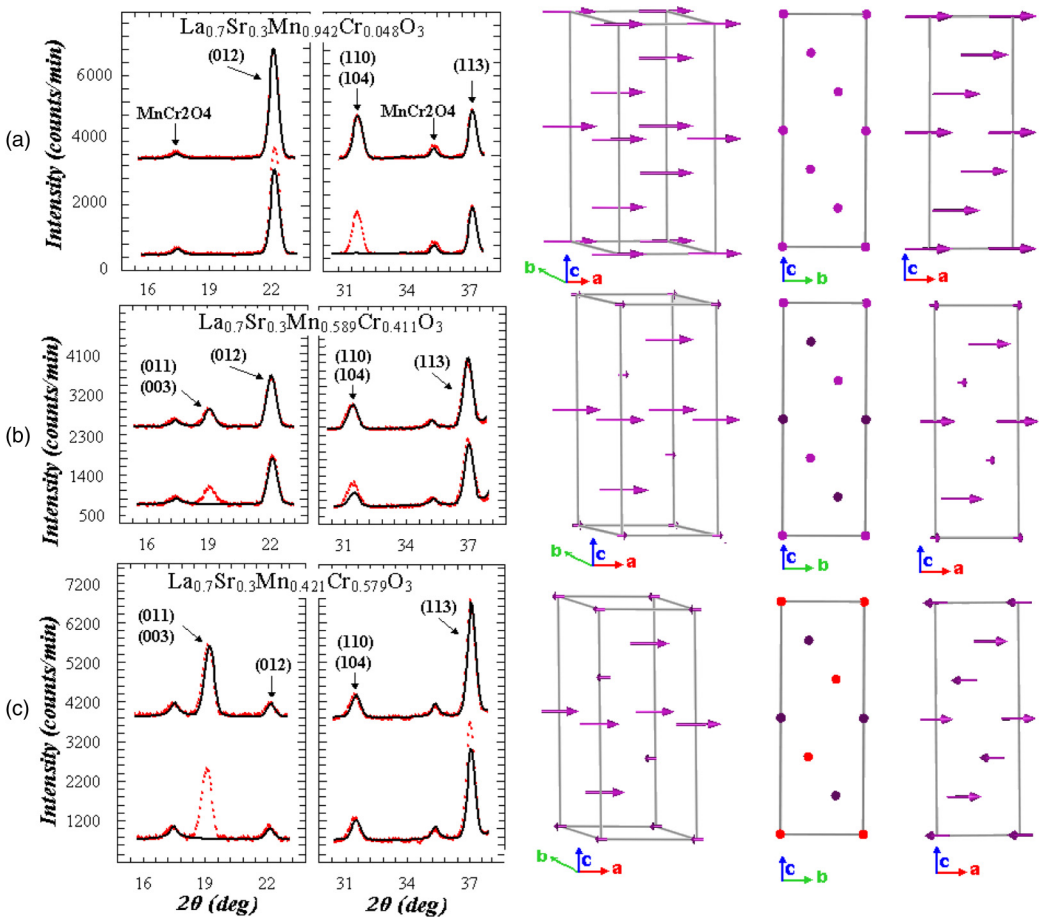

FIG. 4. Select peaks from neutron-diffraction data at 12 K for the (a) $La_{0.7}Sr_{0.3}Mn_{0.942}Cr_{0.048}O_3$, (b) $La_{0.7}Sr_{0.3}Mn_{0.589}Cr_{0.411}O_3$, and (c) $La_{0.7}Sr_{0.3}Mn_{0.421}Cr_{0.579}O_3$ samples. Each row, (a)–(c), contains two plots separated by a break line to focus on the magnetic peaks followed by three plots highlighting the magnetic unit cells. The top curve of each pair of plots contains the nuclear and magnetic phase refined whereas the bottom curve contains only the nuclear phase refined. The top curves of (a) and (c) are offset by 3000 units from the bottom curve whereas the curves in (b) are separated by 2000 units. The respective refined magnetic unit cells are to the right of each pair of plots; the middle magnetic cell plot has the *a* axis out of the page whereas the farthest right cell plot has the *b* axis into the page. The different colored dots in the farthest right figures of (b) and (c) indicate the changed magnetic moments with dark maroon representing arrows coming out of the page whereas red indicates magnetic moments into the page.

At 300 K, for $0.048 \leqslant x \leqslant 0.196$, we find simple ferromagnetic ordering. T_c and the net moment decrease with increasing Cr content. Above $x = 0.196$, the system is paramagnetic at room temperature.

IV. MAGNETIZATION STUDIES

Zero-field-cooled (M_{ZFC}) and field-cooled (M_{FC}) magnetization measurements (Fig. 5) indicate that T_C decreases with increasing Cr content in good agreement with those of Qu *et al.* [28] and Kallel *et al.* [23] for $x < 0.485$. When the samples are cooled in zero field and subsequently warmed to temperatures above T_C with an applied field of 100 Oe, all samples show ferromagnetic behavior immediately below the paramagnetic transition. For $x \geqslant 14.3\%$ an additional antiferromagneticlike transition is seen at lower temperatures.

Upon field cooling and rewarming, all samples exhibit higher magnetization and similar transitions. However, the transitions are less sharp, occur at slightly higher temperatures, and yield larger magnetization, providing evidence that they are very sensitive to small applied fields. They occur at successively higher temperatures with increasing Cr content; 16.9, 25.8, 54.4, 85.1, and 115.4 K for $x = 0.143$, 0.196, 0.221, 0.294, and 0.411, respectively. The $x = 0.062$ sample exhibits the largest low-field magnetization despite a lower saturation than the 0.048 sample (Fig. 6), possibly due to complex interactions between the crystal field and the spin and orbital contributions of the electrons, especially during phase transitions. The $x = 0.062$ and $x = 0.048$ samples exhibit a small discontinuity in the M_{FC} curves near 272 and 287 K, respectively, whereas the $x = 0.062$ sample exhibits the same discontinuity in the M_{ZFC} curve at 287 K. Similar behavior was observed by Sun *et al.* [25].

There is a significant change in magnetization between the $x = 0.143$ to $x = 0.196$ M_{ZFC} and M_{FC} curves, and the $x = 0.196$ curve exhibits lower magnetization than either the $x = 0.143$ or the $x = 0.221$ samples, possibly related to a metal-insulator transition (as observed by Kallel *et al.* [23]), which may alter the coercivity. The M_{ZFC} and M_{FC} curves for $x = 0.411$ exhibit a broad ferromagnetic to paramagnetic

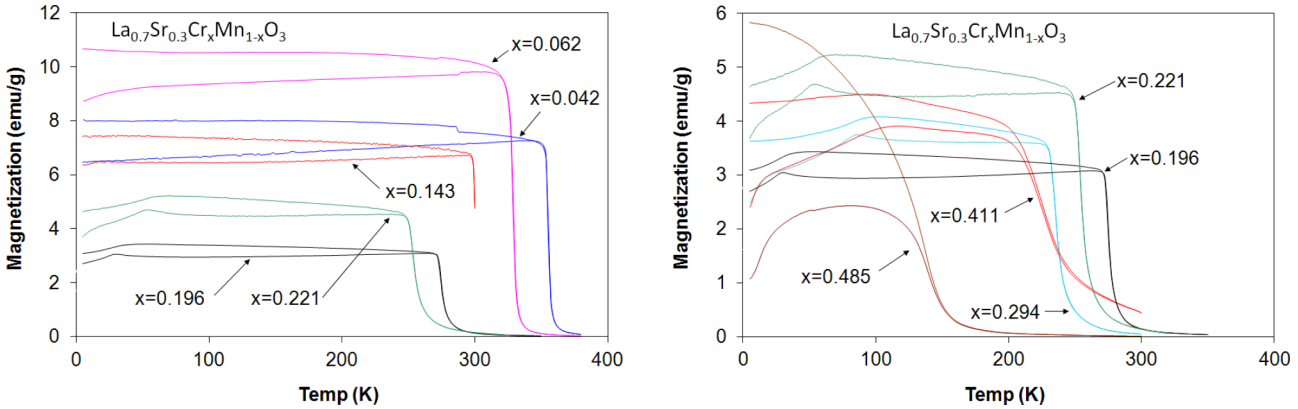

FIG. 5. 100-Oe zero-field-cooled (lower part of curve prior to reaching T_C) and field-cooled (upper part of curve prior to reaching T_C) measurements of magnetization versus temperature for all Cr concentrations. The $x = 0.196$ and 0.221 are common to both for reference purposes. The lower curve for each Cr concentration is the M_{ZFC} curve whereas the upper curve is the M_{FC} curve.

transition with a long tail, extending beyond 300 K. A similar tail at lower temperatures is seen in the $x = 0.485$ sample. This may arise from the competition between the ferromagnetism and the now-dominant antiferromagnetic interactions. Additionally, at this Cr concentration, the amounts of Mn^{3+} and Mn^{4+} are approximately equal (0.289 and 0.3, respectively), a condition optimum for charge ordering. The M_{ZFC} and M_{FC} curves for $x = 0.485$ show the largest difference in magnetization between the M_{ZFC} and M_{FC} curves and a significantly lower T_C. The $x = 0.485$ was also the first sample to exhibit ferrimagnetism in the neutron data.

Magnetization at 5 K versus magnetic field is plotted in Fig. 6. The inset in Fig. 6 shows the saturation magnetization at 5 K versus x. The results are 84.01, 76.12, 69.27, 52.26, 54.97, 48.56, 39.58, and 22.95 emu/g for $x = 0.042$, 0.062, 0.143, 0.196, 0.221, 0.294, 0.411, and 0.485, respectively. The significant reduction in magnetization at $x = 0.196$ coincides with the onset of charge ordering. For $x < 0.485$, all samples reach saturation at fields <25 K Oe. For $x = 0.485$, despite high initial susceptibility, saturation is not reached (Fig. 6), even at a field >75 K Oe. The large difference in saturation magnetization between the $x = 0.143$ and the $x = 0.196$ correlates with a transition from a simple ferromagnet to a charge ordered ferromagnet observed in the neutron data at a composition close to the *M-I* transition [23]. The large difference in saturation magnetization between $x = 0.411$ and $x = 0.485$ correlates with the transition from ferromagnetism to ferrimagnetism.

V. PROPOSED ORDERING

At low Cr concentrations ($x < 0.196$), the results have been modeled (Table II column 9) assuming that the Cr^{3+} ions replace Mn^{3+} [Fig. 7(a)] with reversed spin as suggested by Mahendiran *et al.* [33] and Zhao *et al.* [29] and as we suggested for Ni in our study of $La_{0.7}Sr_{0.3}Mn_{1-x}Ni_xO_3$ [34]. However, the

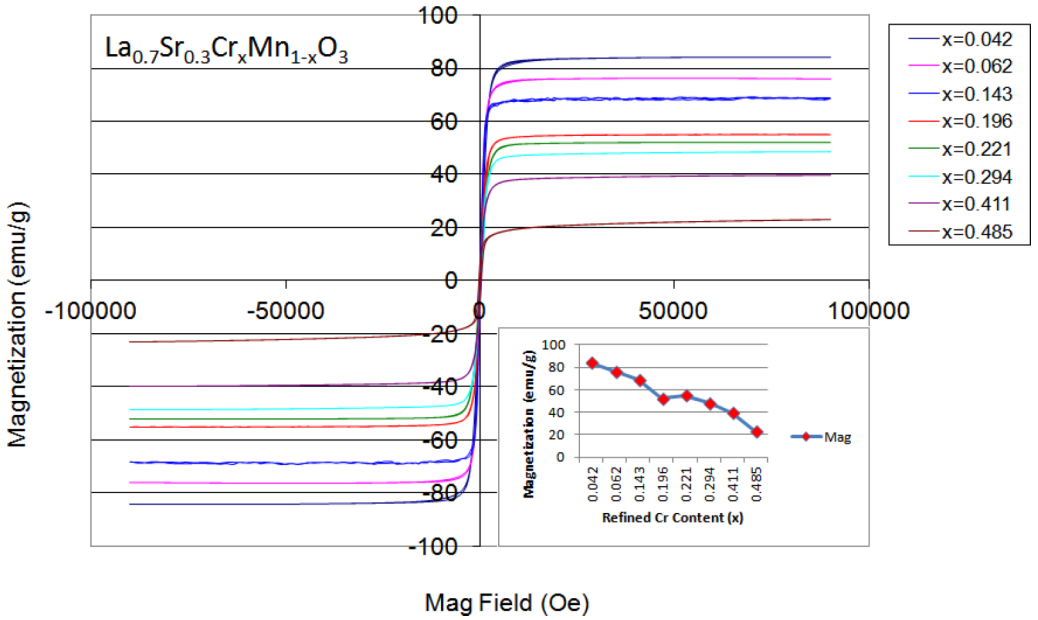

FIG. 6. Magnetization versus magnetic field at 5 K for different Cr concentrations. The inset is a plot of magnetization saturation values versus Cr content.

TABLE II. Calculated and refined magnetic moments (at 12 K) and charge neutrality for all Cr concentrations. Column 1 indicates whether or not the system is refined as a single layer (ferromagnetic) or layered with the layers identified as either *B*1 or *B*2. Column 2 indicates the net charge on the combination of $La^{3+} + Sr^{2+} + O^{2-}$. Columns 3–5 indicate the molar percentage of Mn^{3+}, Mn^{4+}, and Cr^{3+}. Column 6 represents the net charge per layer and is reflective of the degree of charge ordering. Column 7 contains the refined magnetic moments. Column 8 and 9 contain the results of our proposed charge ordered model and the models proposed by both Mahendiran *et al.* [33] and Zhao *et al.* [29].

Layer	Net charge $La^{3+} + Sr^{2+} + O^{2-}$	Molar fraction Mn^{3+}	Molar fraction Mn^{4+}	Molar fraction Cr^{3+}	Net charge per layer	Magnetic moments 12-K refined	Our charge ordered model	Mahendiran *et al.* [33] and Zhao *et al.* [29] models
Parent	−3.300	0.700	0.300			[a]	3.60	3.60
Single	−3.300	0.658	0.300	0.042	0.000	3.130	3.19	3.41
Single	−3.300	0.638	0.300	0.062	0.000	2.950	3.05	3.27
Single	−3.300	0.557	0.300	0.143	0.000	2.480	2.47	2.70
*B*1	−3.300	0.554	0.250	0.196	−0.050	2.550	2.47	
*B*2	−3.300	0.454	0.350	0.196	0.050	1.990	1.93	
*B*1	−3.300	0.532	0.247	0.221	−0.053	2.300	2.41	
*B*2	−3.300	0.426	0.353	0.221	0.053	1.800	1.82	
*B*1	−3.300	0.486	0.220	0.294	−0.080	2.240	2.34	
*B*2	−3.300	0.326	0.380	0.294	0.080	1.290	1.34	
*B*1	−3.300	0.495	0.140	0.365	−0.160	2.630	2.71	
*B*2	−3.300	0.175	0.460	0.365	0.160	0.530	0.61	
*B*1	−3.300	0.453	0.136	0.411	−0.164	2.790	2.67	
*B*2	−3.300	0.125	0.464	0.411	0.164	0.600	0.46	
*B*1	−3.300	0.315	0.200	0.485	−0.100	2.100	2.14	
*B*2	−3.300	0.115	0.400	0.485	0.100	−0.800	−0.76	
*B*1	−3.300	0.085	0.330	0.585	0.030	2.200	2.40	
*B*2	−3.300	0.145	0.270	0.585	−0.030	−1.700	−1.53	

[a]Note—Value from Shirane *et al.* [18].

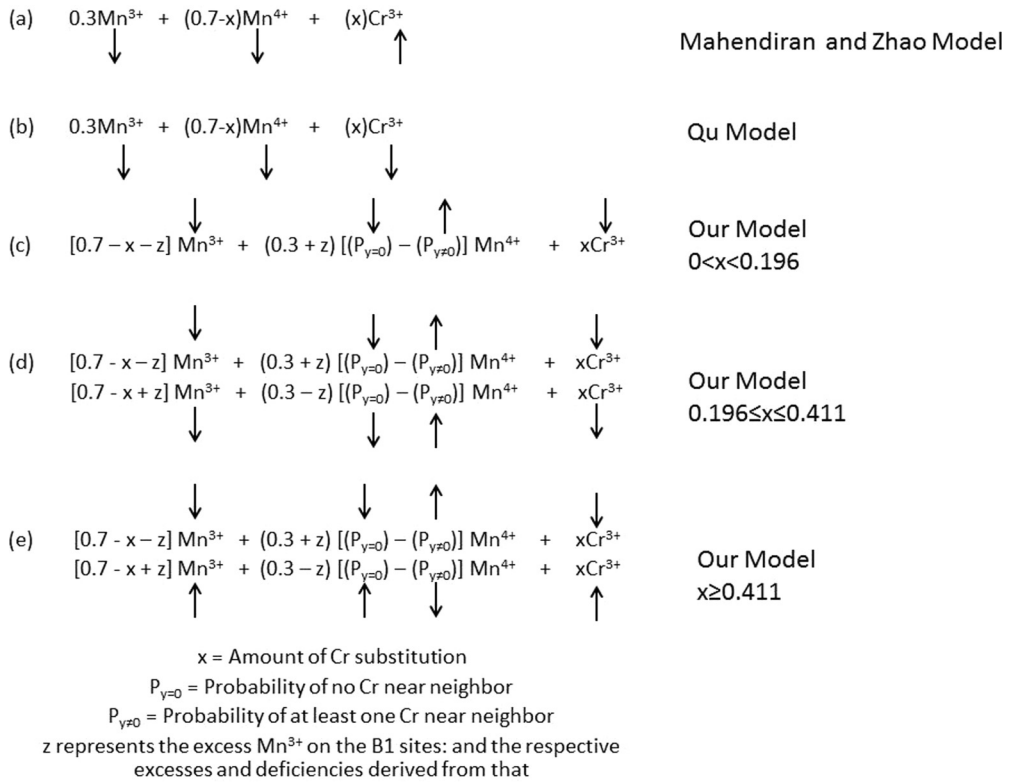

FIG. 7. Possible magnetic ordering schemes: (a) Cr^{3+} replaces Mn^{3+} but with opposite spin, (b) Cr^{3+} replaces Mn^{3+} but with the same spin, (c) Cr^{3+} replaces Mn^{3+} with the same spin but causes Mn^{4+} near neighbors to flip spin; $z = 0$, (d) same as (b) but configured in a charge order ferromagnetic-layered configuration; $z \neq 0$, and (e) same as (b) but in a charge ordered antiferromagnetic-layered configuration; $z \neq 0$.

moments calculated by this model do not decrease as rapidly as found in the neutron data. Qu *et al.* [28] reported that the Cr^{3+} orders ferromagnetically with Mn^{3+} near neighbors when the system is in a ferromagnetic ground state, in agreement with Kanamori-Goodenough superexchange rules (ferromagnetic Mn^{3+}-O-Cr^{3+}) [27,35]. However, Qu *et al.* did not provide an accounting of the Cr^{3+} and Mn^{4+} interactions. Assuming no influence of the Cr ions on the Mn^{4+} ions, this model [Fig. 7(b)] gives an even weaker compositional dependence arising only from the difference in Mn^{3+} ($4\mu_B$) and Cr^{3+} ($3\mu_B$) moments. If the Cr^{3+}-O-Mn^{3+} superexchange is ferromagnetic, we expect the Cr^{3+}-O-Mn^{4+} superexchange to be antiferromagnetic [1,36]. The observed data for $x < 0.196$ are fully explained assuming the spin of the Mn^{4+} ions, which have one or more Cr^{3+} near neighbors will be flipped and align antiparallel to Cr^{3+} and Mn^{3+} [Fig. 7(b)], whereas Mn^{4+} ions with no Cr^{3+} near neighbors are ferromagnetically coupled to Mn^{3+}.

Figure 7 contains the Mahendiran and Zhao model of Mahendiran *et al.* [33] and Zhao *et al.* [29], the model of Qu *et al.*, and our proposed charge ordered model arising by fully considering the effect of Cr on both Mn^{4+} and Mn^{3+} in this system:

(a) Cr^{3+} replaces Mn^{3+} but with opposite spin aligning antiferromagnetically to both Mn^{3+} and Mn^{4+} (Mahendiran *et al.* [33] and Zhao *et al.* [29]).

(b) Cr^{3+} replaces Mn^{3+} and aligns parallel to ferromagnetic Mn (Qu *et al.*)

Our model depicted in Figures 7(c)–7(e) assume that Mn^{4+} ions with Cr neighbors are coupled antiparallel to the Cr ions, which are parallel to Mn^{3+}.

(c) For $x < 0.196$ ferromagnetic double exchange dominates, and a simple ferromagnet is observed.

(d) For $0.196 \leqslant x \leqslant 0.48$ a charge ordered ferromagnetic-layered configuration is observed.

(e) For $x > 0.48$ the Cr^{3+}-O-Cr^{3+} superexchange dominates, leading to a net antiferromagnetic layering (ferrimagnetism).

The probabilities $P_{y=0}$ and $P_{y\neq 0}$ in Figs. 7(c)–7(e) refer to the probability that the Mn species have no Cr near neighbor ($P_{y=0}$) or that they have one or more Cr^{3+} near neighbors ($P_{y\neq 0}$). The concentration of Mn^{4+} ions with n Cr neighbors can be calculated using the binomial theorem and the stoichiometry.

The probability that a given B site has n Cr neighbors is as follows:

$$P(Z=n) = \left(\frac{k!}{n!(k-n)!}\right) p^n q^{(k-n)},$$

where $n = (0{-}6)$ is the number of nearest neighbors, $k = (6)$ is the field of possible nearest neighbors, $p = amount\ of$ Cr, and $q = (1-p)is\ everything\ else$.

At 12 K for $x < 0.196$, the system is best described by Fig. 7(c), a net ferromagnet with Cr^{3+} aligning ferromagnetically with Mn^{3+} near neighbors but flipping the spin of their Mn^{4+} near neighbors. For $0.196 \leq x \leqslant 0.411$ at 12 K, the ordering schema are best described by Fig. 7(d) with charge ordering accounting for the new reflections [(113) and (011) + (003)] seen in the neutron data. The net magnetic behavior for $0.196 \leqslant x \leqslant 0.411$ remains ferromagnetic. For $0.485 \leqslant x < 0.579$ at 12 K, the structure is described by Fig. 7(e); the layers become antiferromagnetically aligned, producing ferrimagnetism. The increasing antiferromagnetic interaction between Cr^{3+} ions breaks the ferromagnetic alignment seen at lower concentrations. Considering the behavior at low Cr concentration, the antiferromagnetic first-neighbor superexchange interaction between Cr^{3+}-O-Mn^{4+} is stronger than the ferromagnetic double exchange between Mn^{3+}-O-Mn^{4+}. The relative strength of the Cr^{3+}-O-Mn^{4+} superexchange and the Cr^{3+}-O-Cr^{3+} superexchange cannot be ascertained, whereas the Mn^{3+}-O-Mn^{4+} double exchange is absent in the insulating region.

At low temperatures and small x ($0 < x < 0.196$), the net ferromagnetic behavior of the system is due to the numerically dominant Mn^{3+}-O-Mn^{4+} ferromagnetic double exchange and random distribution of Cr^{3+} that locally quenches the double exchange. In the intermediate region ($0.196 < x < 0.411$) charge ordering creates a layered structure, and the antiferromagnetic Cr^{3+}-O-Cr^{3+} superexchange continues to drive the system towards an antiferromagnetic state. Above $x \sim 0.411$ the antiferromagnetic Cr^{3+}-O-Cr^{3+} superexchange mechanism dominates whereas charge ordering produces a ferrimagnetic structure in lieu of an antiferromagnetic one.

The results of refined and calculated magnetic moments and charge distribution are presented in Table II. Magnetic moments of $4\mu_B$ for Mn^{3+}, $3\mu_B$ for Mn^{4+}, and $3\mu_B$ for Cr^{3+} are used for the calculations. The calculated net magnetic moments (column 8) for our model are found by considering the probability that Mn^{4+} has one or more Cr^{3+} near neighbors. Column 9 of Table II contains moments calculated using the models of Mahendiran *et al.* [33] and Zhao *et al.* [29] for the simple ferromagnetic samples. Their models clearly underestimate the effect of Cr doping on the moment. For $x > 0.143$ columns 3 and 4 give the Mn^{3+} and Mn^{4+} concentrations in the $B1$ and $B2$ layers derived from the refined moments in the two layers, whereas column 6 gives the net charge on the two layers. For $x \geqslant 0.196$, the table demonstrates the degree of charge ordering within the system.

Wollan and Koehler [17] previously observed the additional (003) + (011) and (113) reflections that correspond to a doubling of the unit cell along the c axis and proposed that the system transitioned from a "*C*"-type to a "*CE*"-type structure. Such ordering was originally proposed by Goodenough [14] as Jahn-Teller distorted or orbital ordering. Wollan and Koehler [17] proposed that excess Mn^{4+} ions from nonstoichiometric $LaMnO_{3+\Delta}$ would occupy the Mn^{3+} sites but with reversed spin. Goodenough [14] further argued that if the Mn^{3+} and excess Mn^{4+} ions formed part of an ordered lattice, double exchange would be inhibited due to a lifting of the degeneracy of Mn^{3+}-O-Mn^{4+} with Mn^{4+}-O-Mn^{3+}, and the ordered state would exhibit high electrical resistivity. In the Cr-substituted system, the Cr^{3+} ion is electronically the same as the Mn^{4+} ion, suggesting the possibility of behavior similar to that of excess Mn^{4+}. Our proposed ordering schema are consistent with that of Wollan and Koehler [17] and Goodenough [14].

On the basis of our refined neutron-scattering data and magnetic measurements, a phase diagram is provided in Fig. 8. The large orange-filled circles are our T_C values extracted from M_{ZFC} magnetic measurements. The hollow circles are the inflection points at temperatures well below T_C, also extracted from M_{ZFC} magnetic measurements. The small

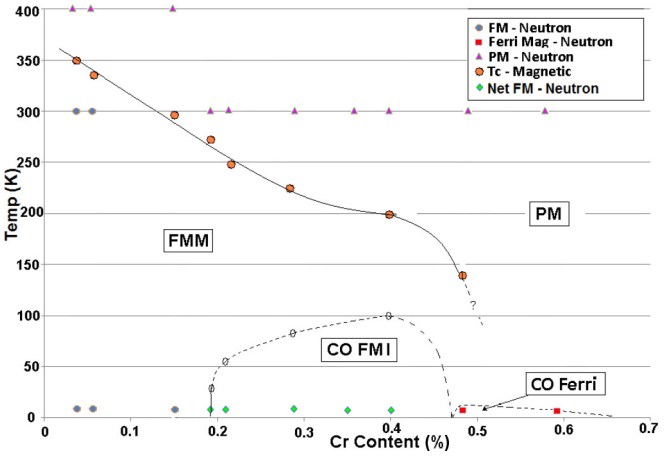

FIG. 8. Phase diagram depicting temperature versus Cr content. Lines are provided as guides and are drawn to fit the results from magnetic data and refined neutron data. The dotted line identifying the antiferromagnetic (AFM) boundary is drawn as a best estimate as we have no data collected at the temperatures necessary to clearly define this boundary. The small round blue-filled, triangular pink-filled, diamond green-filled, and square red-filled data points are neutron data points. The large orange-filled round points are derived T_C transitions from our magnetic data, and the hollow circles are transition points below T_C within our magnetic data. The magnetic phases are as follows: ferromagnetic metal (FMM), ferromagnetic semiconductor (FMS), ferromagnetic insulator (FMI), charge ordered ferromagnetic (CO FM), charge ordered ferrimagnetic (CO FER), AFM, and paramagnetic (PM).

blue-filled circles, green-filled diamonds, red-filled squares, and pink-filled triangles indicate neutron data points. We suggest that the area encompassed by the line passing through the M_{ZFC} inflection points at temperatures less than T_C forms the boundary of charge order, the peak of which occurs at $x = 0.411$, the value at which the quantities of Mn^{3+} and Mn^{4+} are equal. The onset of insulating behavior indicates localization of the charge carriers and is associated with charge ordering.

The transition between the ferromagnetic semimetal to the ferromagnetic insulator [23] correlates with the first appearance of the antiferromagneticlike transitions at temperatures well below T_C observed in the M_{FC} and M_{ZFC} curves. This transition also correlates with a significant change in the slope of the boundary line between the charge ordered ferromagnetic region and the ferromagnetic insulator region and the first observance of the (113) and (011) + (003) reflections. We have also observed similar behavior in our study of the $La_{0.7}Sr_{0.3}Mn_{1-x}Ni_xO_3$ system [37] but occurring over a much reduced span of Ni content.

VI. CONCLUSION

It is suggested that the hierarchy of superexchange interactions (from strongest to weakest) is Cr^{3+}-O-Mn^{4+} (antiferromagnetic), Cr^{3+}-O-Cr^{3+} (antiferromagnetic), and Cr^{3+}-O-Mn^{3+} (ferromagnetic). The first of these induces a flipping of the Mn^{4+} moment for those with Cr^{3+} neighbors whereas the second leads to the system's transition to antiferromagnetic at high Cr concentrations. The third combines with the weakly ferromagnetic Mn^{3+}-O-Mn^{4+} double exchange to preserve the overall ferromagnetic configuration at low Cr concentrations.

If, as assumed, the Cr^{3+}-O-Mn^{4+} superexchange is stronger than the Cr^{3+}-O-Mn^{3+} superexchange, then the magnetic free energy will be lowered if Mn atoms with Cr neighbors are preferentially in the 4+ state. However, this tendency will be opposed by possible charge inhomogeneity, deviating from the random distribution of 4+ charges throughout the system. The double-exchange mechanism that leads to ferromagnetism at low Cr concentrations requires itinerant electrons that can hop from Mn^{3+} ions to Mn^{4+} ions, resulting in metallic conductivity. When Mn ions of either species interact with near-neighbor Cr atoms, however, the superexchange interaction will tend to localize the previously itinerant electrons. We designate the Mn atoms with Cr neighbors as coupled and those with no Cr neighbors as "uncoupled." As the Cr content increases, the concentration of uncoupled Mn ions on the *B* site decreases. The probability that a given *B*-site neighbor is not Cr is $(1\text{-}C_{Cr})$, and so the probability that none of the neighbors are Cr is $(1\text{-}C_{Cr})^6$. To get the concentration of uncoupled Mn ions, we multiply this by the Mn concentration, which is, once again, $(1\text{-}C_{Cr})$. Thus, the concentration of the uncoupled Mn ions is $(1\text{-}C_{Cr})^7$. If the electrical conductivity is solely through first near-neighbor hopping and the Mn electrons are fully localized by one near-neighbor Cr ion, then one would expect the conductivity to vanish when the concentration of uncoupled Mn on the *B* sites reaches the percolation level for a six-coordinate system (31%). This occurs between 15% and 16% Cr. This concentration, rather than corresponding to the metal-insulator point, appears to closely correspond to the appearance of a semimetallic state, which suggests that conductivity may also occur via second near-neighbor hopping. An additional effect must be found to explain the *M-I* transition reported at about 20% Cr [23].

Assuming that Mn ions with two or more Cr near neighbors are exclusively in the 4+ state (up to the stoichiometric limit), the binomial theorem can be used to calculate the point at which the *B*-site Mn ions with two or more Cr near neighbors exceeds 30%—the concentration of Mn^{3+}. This occurs between 21% and 22% Cr, nearly coincident with the reported *M-I* transition point. The remaining uncoupled Mn and weakly coupled Mn (only one Cr neighbor) will all be in the 3+ state and thus incapable of conducting. If this model is correct, then the magnetic and electrical behaviors may be explained by the lower magnetic free energy associated with Cr^{3+}-O-Mn^{4+} superexchange pairs and the effect of localization of the Mn ions by their Cr neighbors. Any discrepancy between the reported *M-I* transition composition and that calculated by the method in use here (less than 2%) may be ascribed to the uncertainty in the exact composition, both with respect to the actual La/Sr ratio, the precise Mn/Cr ratio, and the oxygen stoichiometry. Given these uncertainties, the calculation can be said to predict the observed behavior.

At the same time, the preference of Cr to couple with Mn^{4+} leads to local charge fluctuations, larger than would be expected from a random mixing of 3+ and 4+ ions, with a negative net charge in the "matrix" of the Mn^{3+} ions and

a positive net charge in the Mn^{4+}- (Cr-) rich regions. These fluctuations are the likely drivers of the charge ordering; the formation of supercells which are closer to charge neutral then the randomly distributed negative and positive regions. As the Cr concentration further increases above 21%, Mn^{3+} ions may also have two (or more) Cr neighbors, and the lattice is better able to form the layered structure by preferentially locating Mn^{4+} and Mn^{3+} in alternating layers. The reduced strain at the higher concentration is reflected in the highest-ordering temperature for the charge ordered phase at about 40% Cr when the concentrations of Mn^{3+} and Mn^{4+} are equal.

This model implies that all of the electronic and crystallographic effects are driven by magnetic exchange and that many of the reports of phase separation and compositional inhomogeneity have missed the most essential feature of this and related systems. Neither spin glass nor cluster models are needed to fully describe the observed crystallographic and magnetic behavior. The effect of superexchange on charge localization and the competition between magnetic order and crystallographic order should be calculable. Although it may be very difficult to perform the needed free-energy calculations, it may also be possible to test this model simply by varying the Mn^{4+} concentration (by varying the Sr content) and observing the changes in *M-I* transition and charge ordering compositions.

ACKNOWLEDGMENTS

The authors wish to express their thanks to Dr. J. B. Goodenough of the University of Texas at Austin for his comments and insight into this work and M. Kahveci of the University of Missouri at Columbia for his collection of neutron data. S.K.M. thanks CAPES, Brazil for the award of a fellowship during the course of this work. W.B.Y. would like to thank Dr. A. Yelon for useful discussions.

[1] G. H. Jonker and J. H. Van Santen, Physica **16**, 337 (1950).
[2] M. B. Salamon and M. Jaime, Rev. Mod. Phys. **73**, 583 (2001).
[3] P. Schiffer, A. P. Ramirez, W. Bao, and S.W. Cheong, Phys. Rev. Lett. **75**, 3336 (1995).
[4] L. Brorovskikh, G. Mazo, and E. Kemnitz, Solid State Sci. **5**, 409 (2003).
[5] R. J. H. Voorhoeve, D. W. Johnson, J. P. Remeika, and P. K. Gallagher, Science **195**, 827 (1977).
[6] J. T. Vaughey, J. R. Mawdsley, and T. R. Krause, Mater. Res. Bull. **42**, 1963 (2007)
[7] A. J. Millis, P. B. Littlewood, and B. I. Shraiman, Phys. Rev. Lett. **74**, 5144 (1995).
[8] A. J. Millis, Phys. Rev. B **53**, 8434 (1996).
[9] W. Archibald, J.-S. Zhou, and J. B. Goodenough, Phys. Rev. B **53**, 14445 (1996).
[10] C. Zener, Phys. Rev. **82**, 403 (1951).
[11] H. A. Kramers, Physica **1**, 182 (1934).
[12] H. A. Jahn and E. Teller, Proc. R. Soc. London, Ser. A **161**, 220 (1937).
[13] J. B. Goodenough and A. L. Loeb, Phys. Rev. **98**, 391 (1955).
[14] J. B. Goodenough, Phys. Rev. **100**, 564 (1955).
[15] A. Urushibara, Y. Moritomo, T. Arima, A. Asamitsu, G. Kido, and Y. Tokura, Phys. Rev. B **51**, 14103 (1995).
[16] B. C. Tofield and W. R. Scott, J. Solid State Chem. **10**, 183 (1974).
[17] E. O. Wollan and W. C. Koehler, Phys. Rev. **100**, 545 (1955).
[18] M. M. Shirane, G. Endoh, Y. Hirota, K. Moritomo, and Y. Tokura, Phys. Rev. B **53**, 14285 (1996).
[19] G. H. Jonker and J. H. Van Santen, Physica **19**, 120 (1953).
[20] G. H. Jonker, Physica **22**, 707 (1956).
[21] M. Oishi, K. Yashiro, K. Sato, J. Mizusaki, and T. Kawada, J. Solid State Chem. **181**, 3177 (2008).
[22] O. Z. Yanchevskii, A. G. Belous, A. I. Tovstolytkin, O. I. V'unov, and D. A. Durilin, Inorg. Mater. **42**, 1121 (2006).
[23] N. Kallel, J. Dhahri, S. Zemni, E. Dhahri, M. Oumezzine, M. Ghedira, and H. Vincent, Phys. Status Solidi A **184**, 319 (2001).
[24] N. Kallel, K. Frohlich, M. Oumezzine, M. Ghedira, H. Vincent, and S. Pignard, Phys. Status Solidi C **1**, 1649 (2004).
[25] Y. Sun, W. Tong, X. Xu, and Y. Zhang, Appl. Phys. Lett. **78**, 643 (2001).
[26] W. Li, B. Zhang, W. Lu, Y. Sun, and Y. Zhang, J. Phys. Chem. Solids **68**, 1749 (2007).
[27] J. B. Goodenough, A. Wold, R. Arnott, and N. Menyuk, Phys. Rev. **124**, 373 (1961).
[28] Z. Qu, L. Pi, S. Tan, S. Chen, Z. Deng, and Y. Zhang, Phys. Rev. B **73**, 184407 (2006).
[29] T. S. Zhao, W. X. Xianyu, B. H. Li, and Z. N. Qian, J. Alloys Compd. **459**, 29 (2008).
[30] J. Rodriguez-Carvajal, FULLPROF 2K, Version 3.00, Laboratoire Leon Brillouin-JRC, 2004.
[31] R. D. Shannon, Acta Crystallogr., Sect. A: Cryst. Phys., Diffr., Theor. Gen. Crystallogr. **32**, 751 (1976).
[32] T. F. Creel, J. B. Yang, M. Kahveci, J. Lamsal, S. K. Malik, S. Quezado, B. W. Benapfl, H. Blackstead, O. A. Pringle, W. B. Yelon, and W. J. James, IEEE Trans. Magn. **46**, 1832 (2010).
[33] R. Mahendiran, M. Hervieu, A. Maignan, C. Martin, and B. Raveau, Solid State Commun. **114**, 429 (2000).
[34] T. F. Creel, J. B. Yang, M. Kahveci, J. Lamsal, S. K. Malik, S. Quezado, B. W. Benapfl, H. Blackstead, O. A. Pringle, W. B. Yelon, and W. J. James, in *Materials Research Society Symposium Proceedings of Structural and magnetic properties of* $La_{0.7}Sr_{0.3}Mn_{1-x}Ni_xO_3$(x = 0.05,0.1,0.2,0.3,0.4), edited by J. D. Perkins, A. Ohtomo, H. N. Lee, and G. Herranz, Vol. 1327 (Materials Research Society, San Francisco, CA, 2011), pp. 7–12.
[35] J. Kanamori, J. Phys. Chem. Solids **10**, 87 (1959).
[36] N. Kallel, S. Kallel, A. Hagaza, and M. Oumezzine, Physica B **404**, 285 (2009).
[37] T. F. Creel, J. B. Yang, M. Kahveci, S. K. Malik, S. Quezado,, O. A. Pringle, W. B. Yelon, and W. J. James, J. Appl. Phys. **114**, 013911 (2013).